

Study on the Formation and Characterization of the Intermetallics in Friction Stir Welding of Aluminum Alloy to Coated Steel Sheet Lap Joint

H. DAS, R.N. GHOSH, and T.K. PAL

Multimaterial fabrication such as joining of steel and aluminum is currently prominent in a variety of industries. Friction stir welding is a novel solid-state welding process that causes good joint strength between steel and aluminum. However, the phenomenon contributing significant strength at the interface is not yet clear. In the present study, the interface of the friction stir lap-welded aluminum and coated steel sheet having joint strength maximum (71.4 pct of steel base metal) and minimum, respectively, under two parameter combinations, *i.e.*, 1000 rpm 50 mm min^{-1} and 500 rpm 100 mm min^{-1} , was exclusively characterized by X-ray diffraction, transmission electron microscopy (TEM), concentration profile, and elemental mapping by electron-probe microanalysis. A TEM-assisted EDS study identifies the morphologies of large size $\text{Al}_{13}\text{Fe}_4$ and small size Fe_3Al -type intermetallic compounds at the interface. The diffusion-induced intermetallic growth (thickness) measured from a backscattered image and concentration profile agreed well with the numerically calculated one. The growth of these two phases at 1000 rpm 50 mm min^{-1} is attributed to the slower cooling rate (~ 3.5 K/s) with higher diffusion time (44 seconds) along the interface in comparison to the same for 500 rpm 100 mm min^{-1} with faster cooling rate (~ 10 K/s) and less diffusion time (13.6 seconds). The formation of thermodynamically stable and hard intermetallic phase $\text{Al}_{13}\text{Fe}_4$ at 1000 rpm and travel speed 50 mm min^{-1} in amounts higher than 500 rpm and a travel speed of 100 mm min^{-1} results in better joint strength, *i.e.*, 71.4 pct, of the steel base metal.

DOI: 10.1007/s11661-014-2424-9

© The Minerals, Metals & Materials Society and ASM International 2014

I. INTRODUCTION

RECENTLY, the automotive industry has been concentrating on multimaterial fabrication, which can make vehicles substantially lighter. Adoption of this fabrication in practice is closely linked with the development of efficient methods of joining high-strength-low-alloy steel sheets with competitive structural grades of aluminum alloys.^[1,2] From a practical point of view, both sound joints between dissimilar materials that enable multimaterial design methodologies and low-cost fabrication processes have to be established,^[1-3] but the availability of a sound joining technique for dissimilar materials is indispensable. Joining of dissimilar metals by conventional fusion welding techniques is difficult due to large differences in thermophysical properties such as melting point, thermal conductivity, thermal expansion leading to high distortion, and residual stresses, and also in metallurgical characteristics resulting in the formation of brittle intermetallic phases that generally form by solid-state reaction.^[4] These intermetallic compounds

(IMCs) generally result in mechanical degradation of the joint.^[5,6] This can be avoided possibly by using friction stir welding (FSW), which is a solid-state joining process and does not involve any melting.^[5,6] The use of FSW in the joining of aluminum alloys to steel has recently begun. The feasibility of FSW of aluminum to steel and the importance of an Al/steel interface on weld strength has been considered by numerous authors.^[7-9] The initial investigations on FSW of aluminum alloys to steel reported the presence of IMCs such as $\text{Fe}_4\text{Al}_{13}$, Fe_2Al_5 , and FeAl_4 .^[5,7-9]

However, the effect of such intermetallic phases on the mechanical properties of the weld has not been evaluated.^[5] Tanaka *et al.*^[10] established that the joint strength increased exponentially with a decrease in IMC thickness. A similar opinion was also expressed by Kimapong and Watanabe.^[11] The thickness of the intermetallic layer at the weld interface induced by process parameters such as rotational speed, axial force, and their influence on the degradation of the mechanical properties of the weld joint was reported subsequently by a few researchers.^[10-14] Also, improvement of the joint strength in the IMC layer seems to be necessary, but an IMC layer that is too thick may initiate crack and propagate easily through brittle IMC.^[11] Bozzi *et al.*^[15] reported an optimum IMC layer thickness of 8 μm developed under a rotational speed of 3000 rpm and tool penetration depth of 2.9 mm in friction stir spot welding of aluminum to steel. While making the lap

H. DAS, Senior Research Fellow, and T.K. PAL, Professor, are with the Metallurgical and Material Engineering Department, Welding Technology Centre, Jadavpur University, Kolkata 700032, India. Contact e-mail: tkpal.ju@gmail.com R.N. GHOSH, Professor, is with the Metallurgical and Materials Engineering Department, IIT Kharagpur, Kharagpur, 721302 West Bengal, India.

Manuscript submitted October 24, 2013.

Article published online July 11, 2014

joint of 6063 aluminum alloy (3 mm) to zinc-coated steel sheet (1 mm) using FSW, Das *et al.*^[16] found that a failure load as high as 60 pct of the steel base metal could be achieved. Movahedi *et al.*^[17] studied the friction stir lap welding of 5083 AA and St-12 alloy sheets and reported that rotation speed enhanced joint strength slightly. However, the formation of these intermetallic phases is mainly driven by interdiffusion of the species and is highly dependent on the specific time and temperature history of the welding process. These optimum IMC layer thicknesses depend on welding conditions and specific alloys used. In FSW, due to the introduction of complex deformation and shorter time, the intermetallic phases are thin, making full characterization difficult. The importance of the role of diffusion in the formation of intermetallic phases was studied by the present authors in an earlier investigation.^[16] However, it is not clear how the thermal cycle induced from the process parameters affects the intermetallic phases. Since joints involving this material combination are expected to increase the number of industrial applications, it is important to understand the formation of the intermetallic phases for improved joint performance. Although these recent studies have opened an arena regarding a number of critical issues, a systematic study and a quantitative understanding of the formation of IMCs in friction-stir-welded steel and aluminum alloys is highly desirable.

The main focus of the present work is to examine whether the role of diffusion is worth considering for the formation of IMCs (the size and distribution), since the duration of high-temperature exposure time is short, and also the role of IMCs in the mechanical properties of the joint.

II. EXPERIMENTAL PROCEDURE

FSW of 2.0-mm-thick AA6061 and 1.0-mm-thick high-strength interstitial-free (HIF) galvanized steel sheet was performed in lap joint configuration with the AA6061 sheets on the top using a RM Series Friction Stir Welder (model RM1A-0.7, MTI, USA). A schematic of the dissimilar weld is shown in Figure 1. The FSW machine can be operated with tool rotational speeds up to 3000 rpm, axial load of 67 kN, and plunge rates from 0.1 to 1000 mm min⁻¹. The axial force, torque, and penetration depth values could be recorded simultaneously during each welding operation with the help of the load cell coupled with a data acquisition system. All of the lap welds were made under displacement control mode. *X* force, *Y* force, *Z* force, and torque were recorded for each joint. The tool used was made of steel SKD61 and comprised of a shank, shoulder (11-mm diameter), and probe. A schematic of the tool and pin is shown in Figure 2. The tool shoulder and the pin diameters are 11 and 3 mm, respectively, and the pin length is 2.5 mm. The tool was tilted by 2 deg with the vertical axis in the direction opposite the welding speed. A dwell time of 2 seconds after the complete plunging of the tool pin is maintained for all the experiments. The on-line temperature is monitored at the midlength of the weld assembly using K-type

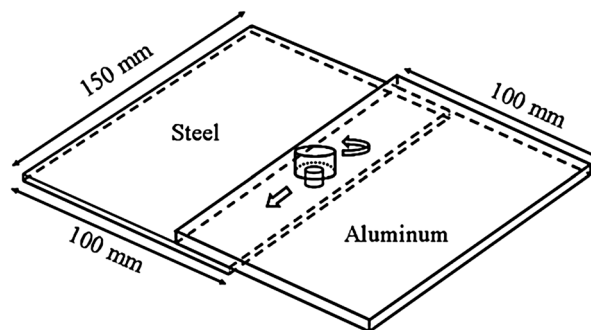


Fig. 1—Schematic of tool-workpiece configuration for friction stir lap welding. The thicknesses of aluminum and steel sheets are 2.0 and 1.0 mm, respectively.

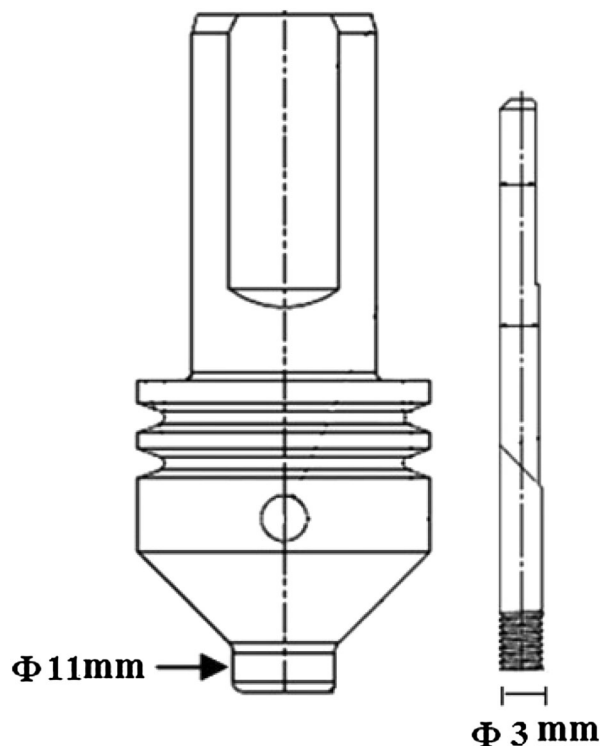


Fig. 2—Schematic of the tool and pin.

thermocouples that are placed at a depth of 0.5 mm from the top surface (*i.e.*, in aluminum sheet and close to the tool shoulder).

The chemical composition and properties of the base material are shown in Table I. Table II provides the welding conditions (rotations per minute and travel speed) used for the Friction stir lap-welded (FSLW) experiments in the present work with respective energy input, process response (*Z* force and torque), and failure load.

The energy^[18] for FSW was calculated using the following expression, and the energy values are summarized in Table II.

$$\text{Energy} = \int_{t=0}^{t=\text{end of welding}} C_z(t) \times \frac{N_p \times 2\pi}{60} dt$$

Table I. Chemical Composition and Mechanical Property of Coated HIF Steel and AA6061

Material	Chemical Composition				Mechanical Properties		
	Pct C	Pct Mn	Pct Si	Pct Ti	YS (MPa)	UTS (MPa)	Failure Load (kN)
Steel	0.0024	0.47	0.094	0.035	225	375	7.0

Material	Chemical Composition				Mechanical Properties		
	Pct Al	Pct Si	Pct Mg	Pct Fe	YS (MPa)	UTS (MPa)	Failure Load (kN)
Aluminum	98.80	0.52	0.91	0.6	172	295	11.8

Table II. Process Parameter, Energy Input, Failure Load, and Respective Process Response

Rotation Speed	Travel Speed (mm min ⁻¹)	Peak Temperature (K)	Energy Input (kJ)	Average Z Force (kN)	Average Torque (Nm)	Failure Load (kN)
500	50	734.2	88.9	6	15	2.4
1000	50	801.7	167.89	4.5	12.8	5
1500	50	829.2	223.8	3.5	11.2	3.3
500	100	685.2	58.6	7	17	2
1000	100	704	109.16	5	13.9	3.2
1500	100	758.6	145	4.5	16	4.1

C_z and N_p represent the respective torque and rotations per minute.

The weld joint tensile strength was evaluated using transverse tensile specimens of size 180 mm × 20 mm in a 100-kN Universal Testing Machine (INSTRON* 8862) at

*INSTRON is a trademark of Illinois Tool Works Inc. (ITW), Glenview, IL.

a crosshead speed of 0.5 mm min⁻¹. The X-ray diffraction (XRD) analysis was carried out using a target of Cu K_α to identify the interfacial IMCs. Nanoindentation experiments were carried out using a fully calibrated NANO INDENTER XP** equipped with a standard Berkovich

**NANO INDENTER XP is a trademark of MTS Systems, Eden Prairie, MN.

indenter. For each loading-unloading cycle, loading and unloading lasted 15 seconds and a dwell time of 30 seconds at each peak load was used, as shown in Figure 3. During each test run, a personal computer collected and stored data for the load and displacement as the indenter was driven into the sample (loading segment) and then withdrawn from it (unloading segment). The raw data were then used to construct the load-displacement plot. Transmission electron microscopy (TEM) was used for the analysis of thin interfacial areas. TEM observations were carried out using a JEOL-2000EX[†] microscope operating

[†]JEOL-2000EX is a trademark of Japan Electron Optics Ltd., Tokyo.

at 200 kV. A 3-mm-disc in the relevant area at the center was punched out from the bulk specimen. The disc was polished down to a thickness less than 100 μ m. The interfacial area was then polished down to 20 μ m using a dimple grinder and diamond pastes. Finally, the interface was thinned by ion beam polishing (GATAN PIPS[‡]).

[‡]GATAN PIPS is a trademark of Gatan, Inc., Warrendale, PA.

III. RESULTS AND DISCUSSION

A. Thermal Cycle Study

Thermal cycle is one of the important factors that determine the formation of the intermetallics and their growth kinetics at the joint interface in spite of short reaction times. However, the thermal cycle and peak temperature measurement for a combination of parameters of the friction-stir-welded dissimilar thick aluminum to steel lap joint are scarce in the literature. Heat is generated due to the friction between the shoulder and workpiece, and that is why the friction coefficient is an important factor; it strongly depends upon the combination of parameters with respective peak temperature. Figure 4 shows that temperatures are higher and thermal cycles are stronger with increasing rotations per minute at travel speeds of 50 and 100 mm min⁻¹ because of the more intense deformational heating consistent with the reduction in frictional heating. With an increase in traverse speed, heat generation and peak temperature decrease.

The data in Table II suggest that the strength of the joint is the highest at 1000 rpm 50 mm min⁻¹ and the lowest at 500 rpm 100 mm min⁻¹. The heat input and peak temperature in the case of the former are higher

than those of the latter. However, characterization was done for both combinations of parameters for better understanding.

B. XRD Analysis of Interface Region

Figure 3 depicts the peak temperature as being around 801.7 K and 685.3 K (528.7 °C and 412.3 °C) along the aluminium-steel interface corresponding to the tool rotational and welding speeds of 1000 rpm, 50 mm min⁻¹ and 500 rpm, 100 mm min⁻¹, respectively. Figures 5(a) and (b) show the XRD analyses of the Fe-Al interface region of the FSLW joints made at tool rotational and welding speeds of 1000 rpm, 50 mm min⁻¹ and 500 rpm, 100 mm min⁻¹, respectively. In Figures 4(a) and (b), the indices (040), (204), (330), (332), and (515) indicate the presence of Al₁₃Fe₄, and the indices (400), (420), (440), and (620) depict the presence of Fe₃Al. It can be noted that the Gibbs free energies for Al₁₃Fe₄ and Fe₃Al phases at 801.7 K and 685.3 K (528.7 °C and 412.3 °C) correspond to -189.2, -178, -79.8 kJ mol⁻¹, and -76.5 kJ mol⁻¹, respectively; thus, the former is thermodynamically more

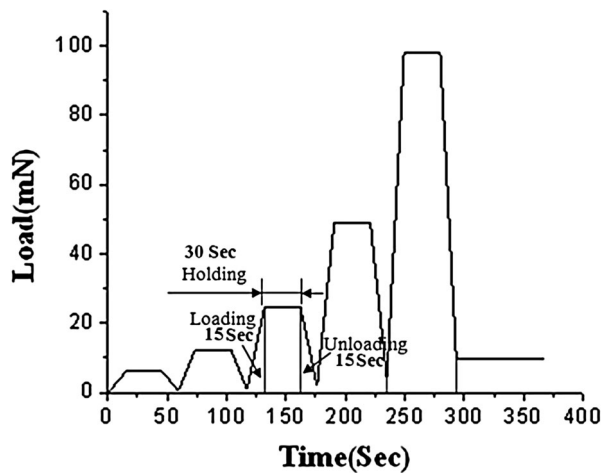
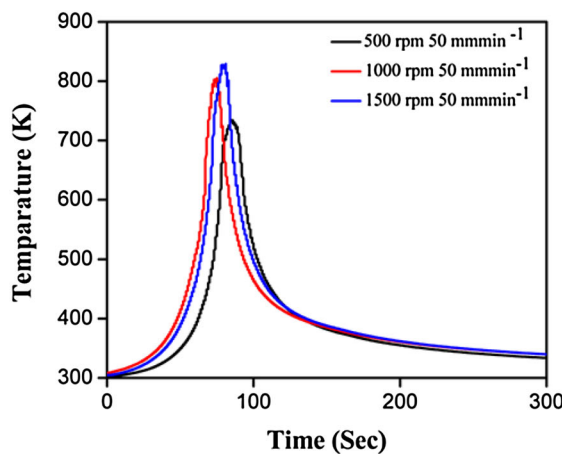


Fig. 3—Load-time sequence in nanoindentation technique.



stable.^[19,20] Therefore, the formation of the Al₁₃Fe₄ intermetallic phase in higher amounts along the interface during FSLW of aluminum to steel is expected, although Al₁₃Fe₄ and Fe are expected to react with each other to transform partially to Fe₃Al.

A comparison of Figures 5(a) and (b) indicates a greater presence of Al₁₃Fe₄ phase at higher tool rotational speed (1000 rpm) and lower welding speed (50 mm min⁻¹) in comparison to the same at lesser rotational speed (500 rpm) and greater welding speed (100 mm min⁻¹). The greater extent of Al₁₃Fe₄ phase at higher rotational speed and lower welding speed can be attributed to the smaller cooling rate (~3.5 K/s) along the interface in the temperature range of 523 to 623 K (250 to 350 °C) in comparison to the same at lesser rotational speed and higher welding speed (~10 K/s).^[21]

C. Prediction of Diffusion Distance Numerically and Correlation with Electron-Probe Microanalysis Concentration Profile and IMC Thickness Measured from Scanning Electron Microscopy Images

The concentration profiles of Al and Fe across the joint were examined for both cases by electron-probe microanalysis (EPMA), as shown in Figures 6(a) and (b). The inset of these figures shows the widths of the interface measured using the boundary condition^[22]:

$$\text{Boundary shift } (\varepsilon_f) = (\text{area of } A + \text{area of } B)/100, \quad [1]$$

where the ε_f values are 0.75 and 0.451 μm^2 at 1000 rpm 50 mm min⁻¹ and 500 rpm 100 mm min⁻¹, respectively.

Figures 5(c) and (d) show scanning electron microscopy (SEM) backscattered images, where the average widths of the interfaces of the two joints were measured critically and are 6.5 and 4.2 μm , respectively.

If diffusion plays a major role in the development of the interface, its width should be proportional to \sqrt{Dt} , where D is the diffusivity and t is the diffusion time at a particular temperature (T). The diffusivity of Al in Fe ($D_{\text{Al}}^{\text{Fe}}$) is given by^[23]

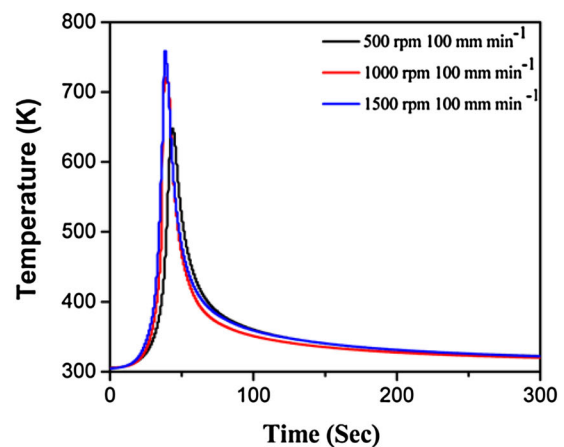


Fig. 4—Thermal cycle for different combinations of parameters.

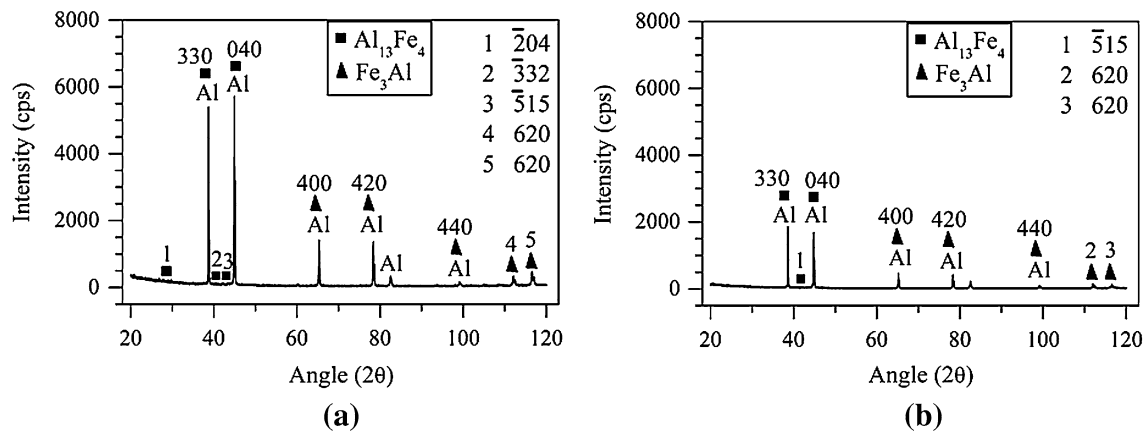


Fig. 5—XRD pattern at FSLW joint interface made at tool rotational speeds and welding speeds of (a) 1000 rpm, 50 mm min⁻¹ and (b) 500 rpm, 100 mm min⁻¹.

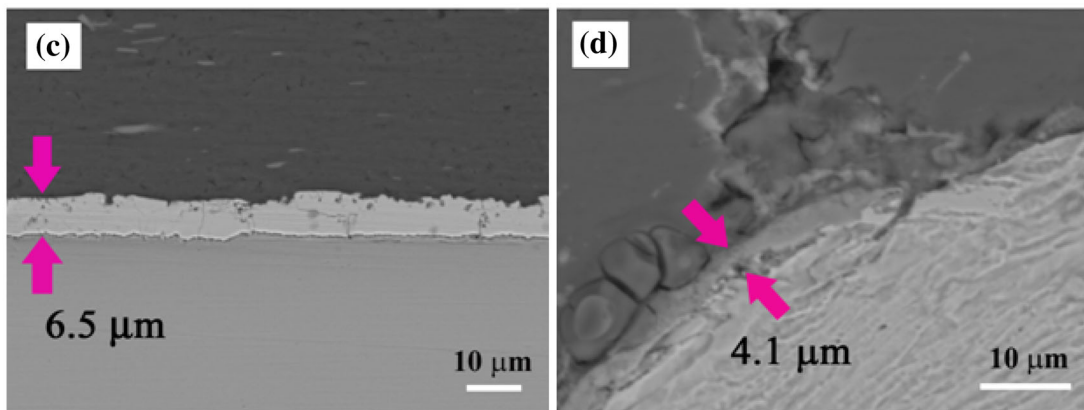
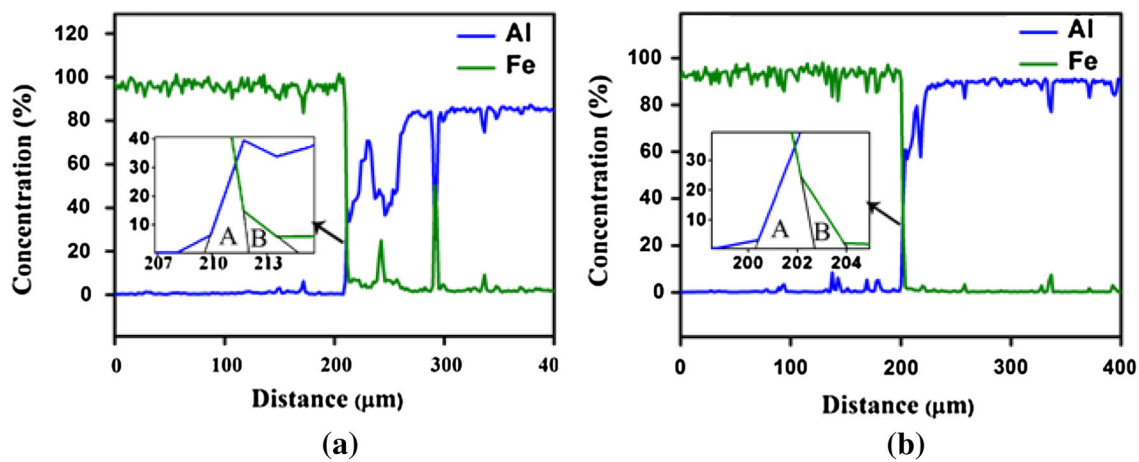


Fig. 6—Concentration profile measurement by EPMA for (a) 1000 rpm and travel speed 50 mm min⁻¹ (inset: boundary shift measurement shown) and (b) 500 rpm and travel speed 100 mm min⁻¹ (inset: boundary shift measurement shown). IMC thickness measured by SEM backscattered imaging for (c) 1000 rpm and travel speed 50 mm min⁻¹ and (d) 500 rpm and travel speed 100 mm min⁻¹.

$$D_{Al}^{Fe} = 2.5 \times 10^{-14} \exp\left(-\frac{30,586}{RT}\right) \text{ cm}^2/\text{s} \quad [2]$$

In the preceding expression, T denotes temperature in kelvin and R is the universal gas constant.

The ratio of the widths of the interfaces at the two parameters can be estimated by calculating the diffusion times from the thermal profile (Figure 4). The diffusion times for 1000 rpm 50 mm min⁻¹ and 500 rpm 100 mm min⁻¹ are 44 seconds (t_1) and 13.6 seconds (t_2), respectively, at 523 K (250 °C). The following expression

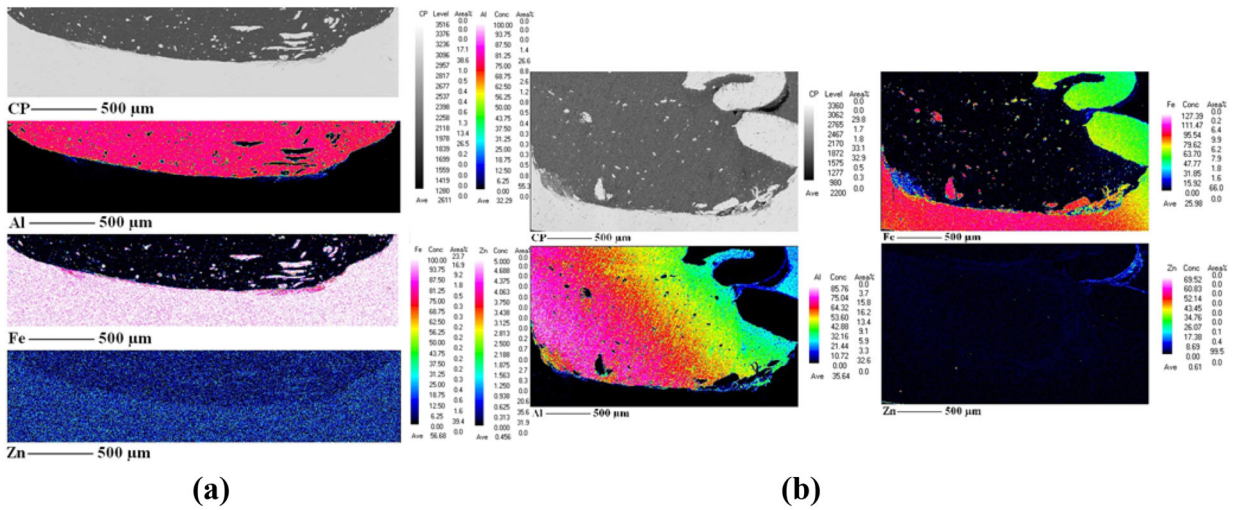


Fig. 7—Elemental mapping (Fe, Al, and Zn) by EPMA for (a) 1000 rpm and travel speed 50 mm min⁻¹ and (b) 500 rpm and travel speed 100 mm min⁻¹.

shows that diffusion of Al in Fe is responsible for the formation of bond.

$$\left(\frac{X_1}{X_2}\right)_{Al} = \sqrt{(D_{Al}^{Fe}) \frac{t_1}{t_2}} = 1.79 \quad [3]$$

The numerical values for the ratio were obtained by substituting the values of the diffusion time at the two parameters. The corresponding magnitude of the ratio obtained from SEM backscattered images in Figures 6(c) and (d) is 6.5/4.1 = 1.58 and that obtained by boundary shift measurement from the concentration profiles given in Figures 6(a) and (b) is 0.75/0.451 = 1.66. These findings suggest that the calculated ratio obtained by assuming aluminum to be the diffusing species in iron is in excellent agreement with the measured ratio of the interface widths. Therefore, the diffusion of aluminum in the iron matrix is primarily responsible for the evolution of the structures within the interface.

D. EPMA Analysis of the Interface Region

Further, a close look into the interface region revealed a fine distribution of particles identified as iron rich (Figures 7(b) and (c)); due to the rubbing action of the tool, iron particles are embedded into the aluminum matrix. The IMCs were found only at the interface. Again, a uniform layer of Zn along the entire interface of the lap joint was observed under parameter 1000 rpm 50 mm min⁻¹, whereas such Zn layer was absent under parameter 500 rpm 100 mm min⁻¹. The zinc coat on the surface of the steel is basically composed of iron-zinc IMC, which firmly holds the zinc with steel.^[13] During friction stir welding, the metal in the lap interface undergoes the synthetic effect of the thermal cycle and mechanical cycle because of the action of friction, stir, and extrusion of the tool. The peak temperature experienced at the interface of the lap joint under parameter 1000 rpm 50 mm min⁻¹ leads to melting of

zinc due to its lower melting point [693 K (420 °C)], and high pressure simultaneously results in the rupture of surface oxide films at both sheet surfaces and also extrudes the liquid zinc with broken oxide film, which spreads along the interface between the two sheets.^[13] In this way, Al and steel are tightly extruded together after the liquid Zn is pushed out.

E. TEM Study at the Interface

TEM with a selected area diffraction (SAD) pattern for the interface region for two different friction-stir-welded joints is shown in Figures 8(a) through (d), (e1), (e2), and (f) through (h). A distinct difference was clearly observed between the spotty^[24] and ring-type SAD pattern of the aluminum base metal and the interface of the two friction-stir-welded joints. The SAD pattern of the joint interface is similar to the polycrystalline material, indicating the presence of intermetallic phases. TEM-assisted EDS analysis confirms the presence of Al₁₃Fe₄ and Fe₃Al intermetallic phases. SAD pattern also clearly identifies the presence of these two intermetallics. In Figures 8(d) and (h), the indices (204), (332), and (515) indicate the presence of Al₁₃Fe₄ and the index (620) reveals the presence of Fe₃Al. The measured interplane angle (106.7 deg) shown in the inset of Figure 8(d) is more or less close to the calculated angle (107.6 deg) of the Al₁₃Fe₄ monoclinic system.

Diffusion of aluminum in iron is likely to occur, which promotes Al₁₃Fe₄ (thermodynamically more favorable) IMC formation due to the fact that a small amount of Fe atom should diffuse in Al-rich compositions to form monoclinic Al₁₃Fe₄. On the other hand, Al₁₃Fe₄ and Fe are expected to react with each other to transform kinetically favored Fe₃Al due to less mutual diffusion of aluminum and iron, which promotes vacancy less structure. The diffraction pattern in the 1000 rpm 50 mm min⁻¹ combination parameter is similar to that of the fine-grain standard aluminum,^[24] which implies a higher degree of grain refinement in 1000 rpm and

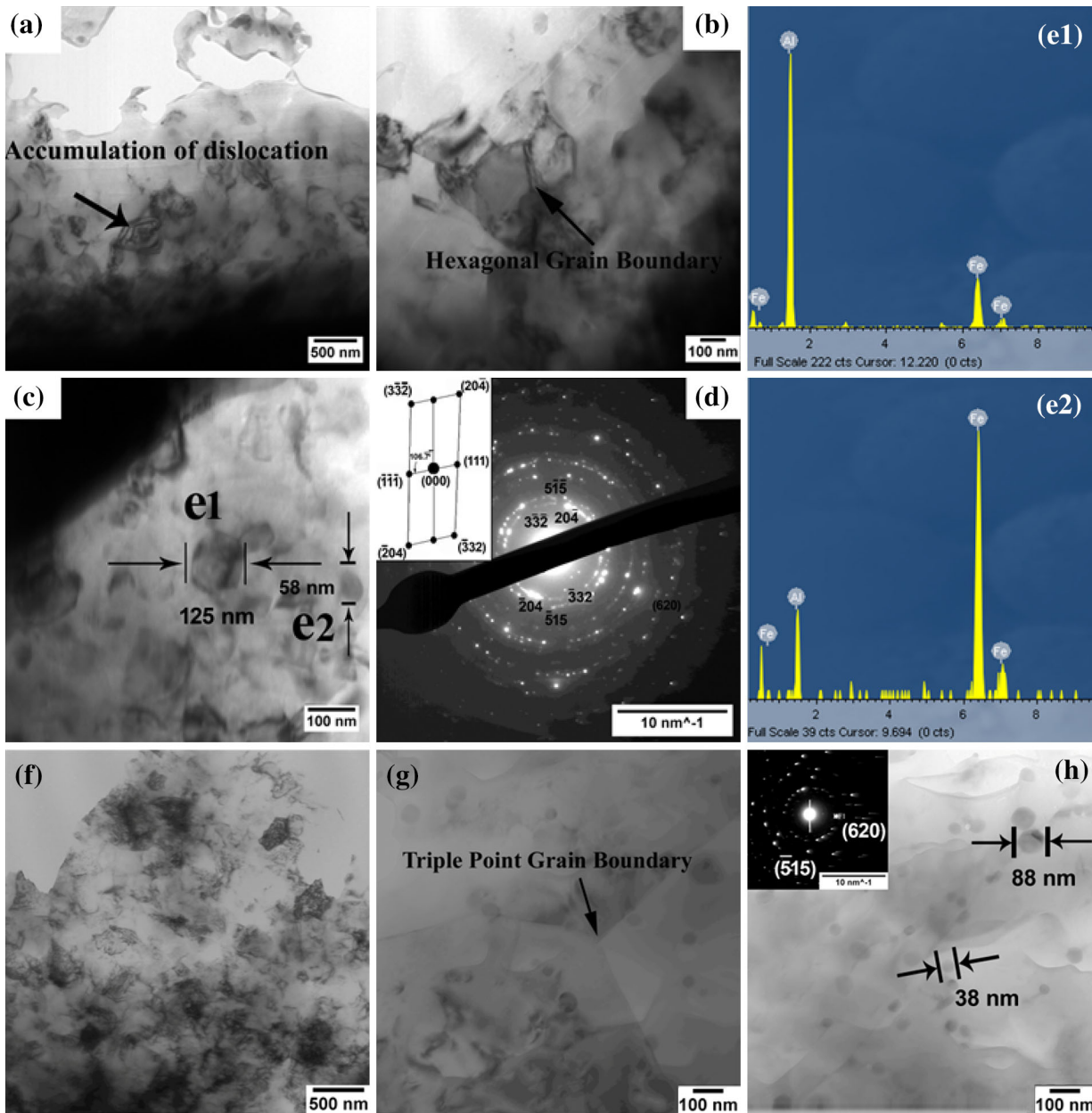


Fig. 8—High-resolution TEM images for 1000 rpm and travel speed 50 mm min^{-1} : (a) joint interface, (b) hexagonal type of grains, (c) size measurement for two types of intermetallics named e1 (125 nm) and e2 (58 nm), (e1) TEM-assisted EDS analysis for e1-type intermetallic identified as $\text{Al}_{13}\text{Fe}_4$, (e2) TEM-assisted EDS analysis for e2-type intermetallic identified as Fe_3Al , (d) SAD pattern for two types of intermetallic (inset: angle measured from the selected point of the pattern indicating monoclinic $\text{Al}_{13}\text{Fe}_4$) high-resolution TEM images for 500 rpm and travel speed 100 mm min^{-1} , (f) interface, (g) triple-point grain boundary, and (h) size measurement for two types of intermetallics, *i.e.*, 88 nm ($\text{Al}_{13}\text{Fe}_4$) and 38 nm (Fe_3Al) (confirmed from EDS) (inset: SAD pattern).

50 mm min^{-1} than in 500 rpm and 100 mm min^{-1} . 1000 rpm 50 mm min^{-1} has higher energy input than 500 rpm 100 mm min^{-1} . However, the interesting thing in FSW is that process response plays a predominate role in determining energy input. The energy input varies from 58.6 kJ for parameter 500 rpm 100 mm min^{-1} (Z force 7 kN and torque 17 Nm) to 223.8 kJ for parameter 1500 rpm 50 mm min^{-1} (Z force 3.5 kN and torque 11.2 Nm). For a particular rotations per minute value, as the travel speed increases, the peak temperature decreases; in that case, the probability of sliding

increases. Due to the fact that there is less heat generation in 500 rpm and 100 mm min^{-1} , the materials are not properly softened, which is reflected in the increased force and torque values. The steady flow of material around the welding tool during FSW is closely linked to the sound joint, *i.e.*, the optimized parameter 1000 rpm 50 mm min^{-1} (Z force 4.5 kN and torque 12.8 Nm) with energy input of 167.8 kJ. The process response for 1000 rpm and 50 mm min^{-1} is itself a clear indication of optimum recrystallization at the optimum energy input; as a result, the grain size is finer than

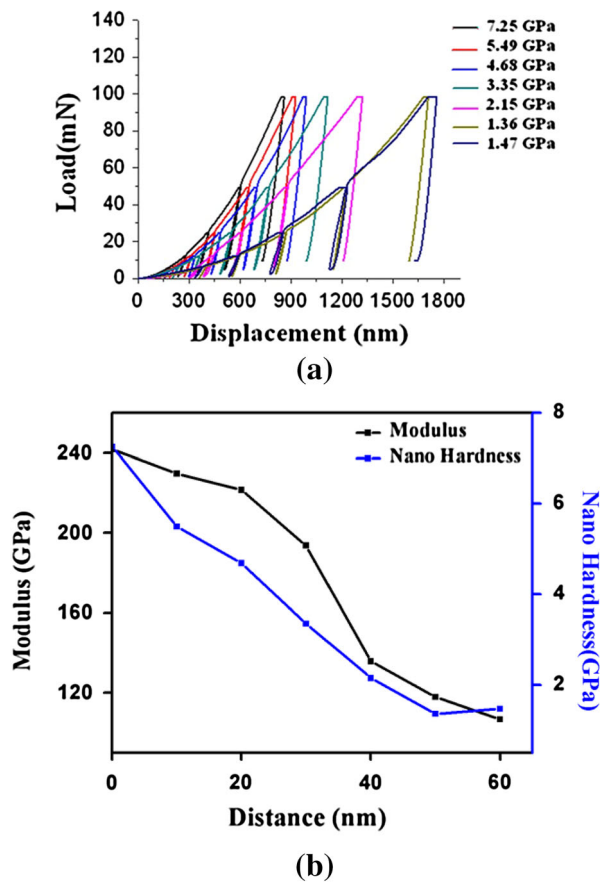


Fig. 9—(a) Load vs displacement curve and (b) nano hardness vis-à-vis modulus curve for 1000 rpm and travel speed 50 mm min^{-1} .

$500 \text{ rpm } 100 \text{ mm min}^{-1}$. Interestingly, hexagonal types of grains (Figure 8(b)) with some accumulation of dislocations are also observed in Figure 8(a). The triple-point grain boundary for 500 rpm and 100 mm min^{-1} is shown in Figure 8(g).

The size of the large intermetallic phase, identified as $\text{Al}_{13}\text{Fe}_4$, is close to 125 nm (EDS analysis shown in Figure 8(e1)), and that of the small size intermetallic, identified as Fe_3Al , is close to 58 nm (EDS analysis shown in Figure 8(e2)) in $1000 \text{ rpm } 50 \text{ mm min}^{-1}$, as shown in Figure 8(c). Whereas in $500 \text{ rpm } 100 \text{ mm min}^{-1}$ large intermetallics, identified as $\text{Al}_{13}\text{Fe}_4$, are close to 88 nm , small size intermetallics, identified as Fe_3Al , are close to 38 nm , as shown in Figure 8(h). The growth of these two phases at $1000 \text{ rpm } 50 \text{ mm min}^{-1}$ can be attributed to the slower cooling rate ($\sim 3.5 \text{ K/s}$) with higher diffusion time (44 seconds) along the interface in comparison to the same for $500 \text{ rpm } 100 \text{ mm min}^{-1}$ with faster cooling rate ($\sim 10 \text{ K/s}$) and lower diffusion time (13.6 seconds).

F. Nanoindentation Study at the Interface

The nanoindentation technique was successfully used to understand quantitatively the effect of nanosize intermetallics on mechanical properties. It is difficult to examine the exact details of the microstructural

features in the vicinity of the indentation site, but some useful information may be obtained by comparing the load-displacement ($P-h$) curves measured at different positions in the specimen surface. The loading-unloading cycles obtained from the $P-h$ curves, as presented in Figure 8 for an rpm 1000 and travel speed 50 mm min^{-1} parameter, can provide a comparison between the material responses at different positions of the surface. Figure 9(a) indicates that point 2 deformed much more easily than point 1, point 3 deformed much more easily than point 2, and so on. At points 6 and 7, however, more or less the same type of deformation was observed. The resultant unloading and reloading curves nearly coincided for points 1 to 5, as shown in Figure 9(a), indicating elastic behavior, whereas distinct hysteresis loops for points 6 and 7 were observed in the unloading-reloading cycles, indicating reverse plasticity. The results are expected because indentations 6 (138.7 Hv) and 7 (150 Hv) represent steel that has undergone deformation. On the other hand, the nano hardness values at other points such as point 1 (739.5 Hv) for $\text{Al}_{13}\text{Fe}_4$ and points 2 (560 Hv), 3 (477.4 Hv), 4 (402 Hv), and 5 (219.3 Hv) for Fe_3Al represent the zone of nondeformation. A similar type of nano hardness for these two different types of intermetallics was reported by previous researchers.^[25] A close look at Figure 8(b) clearly reveals that the nano hardness and elastic modulus representing the material property (inhomogeneity) show the same trend.

IV. CONCLUSIONS

1. The lap joint of 6061 aluminum alloy (2 mm) to a zinc-coated steel sheet (1 mm) can be successfully made by the FSW process, and a failure load as high as 71.4 pct of the steel base metal can be achieved.
2. The average joint strength is significantly influenced by the thermal cycle and combined effect of rotational speed and travel speed as well as energy input. The optimized parameter 1000 rpm and travel speed 50 mm min^{-1} with energy input and peak temperature contribute to high-performance joint.
3. The formation of thermodynamically stable and hard intermetallic phase $\text{Al}_{13}\text{Fe}_4$ at 1000 rpm and travel speed 50 mm min^{-1} in higher amounts than 500 rpm and travel speed 100 mm min^{-1} contributes to better joint strength.
4. The diffusion-induced intermetallic thickness measured from a backscattered image and concentration profile agreed well with the numerically calculated one, confirming that diffusion plays a predominate role.
5. A TEM-assisted EDS study identified the morphologies of large size $\text{Al}_{13}\text{Fe}_4$ and small size Fe_3Al . The growth of these two phases at $1000 \text{ rpm } 50 \text{ mm min}^{-1}$ is attributed to the slower cooling rate ($\sim 3.5 \text{ K/s}$) with higher diffusion time (44 seconds) along the interface in comparison to the same for $500 \text{ rpm } 100 \text{ mm min}^{-1}$ with faster cooling rate ($\sim 10 \text{ K/s}$) and less diffusion time (13.6 seconds).

ACKNOWLEDGMENTS

The financial support of the CSIR (New Delhi, India) for this work is gratefully acknowledged. The authors are very much thankful to Dr. G. Das, Principal Scientist, Mechanical Division, National Metallurgical Laboratory, Jamshedpur, and Drs. A. Dasgupta, A. Kumar, and T. Jayakumar, Metallurgy and Materials Group, Indira Gandhi Centre for Atomic Research (IGCAR, Kalpakkam, India), for extending their facility for EPMA and TEM.

REFERENCES

1. T. DebRoy and H.K.D.H. Bhadeshia: *Sci. Technol. Weld. Join.*, 2010, vol. 15, pp. 266–70.
2. T.A. Barnes and I.R. Pashby: *J. Mater. Process. Technol.*, 2000, vol. 99, pp. 62–71.
3. S.H.C. Park, Y.S. Sato, and H. Kokawa: *Proc. 7th Int. Symp., JWS*, Kobe, Japan, 2001, pp. 639–44.
4. V.R. Ryabov: Foreign Technology Division, Wright-Patterson Air Force Base, OH, 1973, p. 16.
5. A. Elrefaey, M. Gouda, M. Takahashi, and K. Ikeuchi: *J. Mater. Eng. Perform.*, 2005, vol. 14, pp. 10–17.
6. Maruzen, ed.: *Welding Handbook*, Japan Welding Society, Tokyo, 1990, p. 496.
7. M. Aritoshi and K. Okita: *Q. J. Jpn Weld. Soc.*, 2002, vol. 71, pp. 432–36.
8. K. Ikeuchi, N. Yamamoto, M. Takahashi, and M. Aritoshi: *Trans. JWRI*, 2005, vol. 34, pp. 1–9.
9. W. Lee, M. Schmuecker, U.A. Mercardo, G. Biallas, and S. Jung: *Scripta Mater.*, 2006, vol. 55, pp. 355–58.
10. K. Tanaka, M. Kumagai, and H.J. Yoshida: *Jpn. Inst. Light Met.*, 2006, vol. 56, pp. 317–22.
11. K. Kimapong and T. Watanabe: *Mater. Trans. JIM*, 2005, vol. 46, pp. 835–41.
12. T. Watanabe, H. Takayama, and A. Yanagisawa: *J. Mater. Proc. Technol.*, 2006, vol. 178, pp. 342–49.
13. Y.C. Chen and K. Nakata: *Metall. Mater. Trans. A*, 2008, vol. 39A, pp. 1985–92.
14. H. Uzun, C.D. Donne, A. Argagnotto, T. Ghidini, and C. Gambaro: *Mater. Des.*, 2005, vol. 26, pp. 41–46.
15. S. Bozzi, A.L.H. Etter, T. Baudin, B. Criqui, and J.G. Kerbiguet: *Mater. Sci. Eng. A*, 2010, vol. 527, pp. 4504–09.
16. H. Das, S. Basak, G. Das, and T.K. Pal: *Int. J. Adv. Manufact. Technol.*, 2013, vol. 64, pp. 1653–61.
17. M. Movahedi, A.H. Kokabi, S.M. Seyed Reihani, and H. Najafi: *Sci. Technol. Weld. Join.*, 2012, vol. 17, pp. 162–68.
18. S. Zimmer, L. Langlois, J. Laye, and R. Bigot: *Int. J. Adv. Manufact. Technol.*, 2010, vol. 47, pp. 201–15.
19. R. Pretorius, A.M. Vredenberg, and F.W. Saris: *J. Appl. Phys.*, 1991, vol. 70, pp. 3636–46.
20. R. Pretorius, R. de Reus, A.M. Vredenberg, and F.W. Saris: *Mater. Lett.*, 1990, vol. 9, pp. 494–99.
21. H. Das, S.S. Jana, T.K. Pal, and A. De: *Sci. Technol. Weld. Join.*, 2014, vol. 19, pp. 69–75.
22. N. Lee and J. Cahoon: *J. Phase Equilib. Diff.*, 2011, vol. 32, p. 226.
23. J. Hirvonen and J. Raisanen: *J. Appl. Phys.*, 1982, vol. 53, p. 3314.
24. J.W. Edington: *Practical Electron Microscopy in Material Science*, Van Nostrand Reinhold, New York, 1976.
25. M. Potesser, T. Schoeberl, H. Antrekowitsch, and J. Bruckner: *EPD Congress*, TMS, Warrendale, PA, 2006, pp. 167–176.